Available online at www.sciencedirect.com
ScienceDirect
International Journal of Heat and Fluid Flow 28 (2007) 909–921
International Journal of HEAT AND FLUID FLOW
www.elsevier.com/locate/ijhff

Validation of large-eddy simulation of strongly curved stationary and rotating U-duct flows

K.M. Guleren *, A. Turan

School of MACE, University of Manchester, George Begg Building, Sackville Street, P.O. Box 88, Manchester M60 1QD, United Kingdom

Received 15 February 2006; received in revised form 3 November 2006; accepted 3 November 2006
Available online 12 February 2007

Abstract

Numerical predictions of the developing turbulent flow through stationary and rotating U-ducts with strong curvature are presented using large-eddy simulation (LES). The primary aim is to validate LES in a strongly curved U-duct for three different cases: stationary (non-rotating), positive and negative rotational cases. Selected flow models have provided a challenging test for the methodology adopted in terms of boundary conditions, wall functions and subgrid-scale (SGS) models, which are still regarded as crucial research topics within the context of LES. The agreement between the predictions and experimental data is quite satisfactory considering the coarse grid adopted. Discrepancies are observed to diminish near the lateral walls due to the relatively fine grid resolution. It is seen that LES performs better than the two-component-limit (TCL) RANS model in predicting the quantitative features of the turbulent flow through a U-duct with a non-conforming mesh adaptation.

Keywords: Large-eddy simulation; Strong curvature; U-duct; Rotation; Non-conforming mesh

1. Introduction

Today's modern design techniques have an important role to play in the safety and efficiency of turbomachines. Flows in turbine internal cooling passages and radial impellers are prime examples where the centrifugal and Coriolis forces display dominant influences on the flow behaviour. In internal cooling flow problems, cool air coming from the compressor stages is guided through the complex passages within the turbine blades, where the flow encounters sharp bends. In the radial impeller, highly-curved blades (either twisted or untwisted) transport the axial flow to the radially oriented diffuser (either vaned or vaneless) by increasing the kinetic energy and pressure of the flow. In this paper, the chosen flow problem builds upon the basic understanding of the internal cooling passage flow within the stationary U-duct geometry with the hope that there are strong similarities with the radial impeller flow incorporating rotation. For example, in a low-speed centrifugal compressor, the pressure side of the impeller blade is concave in shape till half way along the meridional shroud (or hub) length and then turns into a convex shape along the remainder. Similarly, in the bend of a U-duct, the pressure side becomes the concave-shaped outer wall in the positive rotation and the convex-shaped inner wall in the negative rotation.

In spite of the wide range of industrial applications, and documented numerical and experimental contributions, it is still difficult to accept that for many advanced flow devices the "best design" has been currently achieved or will be in the near future. A significant number of these contributions relevant to improving the internal cooling of gas-turbine blades and to enhancing the efficiency of centrifugal compressors has recently been reviewed by Iacovides and Launder (2006) and Krain (2005), respectively.

* Corresponding author. Present address: Cumhuriyet University, Faculty of Engineering, Mechanical Engineering Department, 58140 Sivas, Turkey.
E-mail addresses: M.Guleren@postgrad.manchester.ac.uk, melihguleren@cumhuriyet.edu.tr (K.M. Guleren), A.Turan@manchester.ac.uk (A. Turan).

0142-727X/$ - see front matter © 2007 Elsevier Inc. All rights reserved.
doi:10.1016/j.ijheatfluidflow.2006.11.010

Nomenclature

$\in_{ij3}$	Levi-Civita's alternating tensor
k	turbulent kinetic energy
t	time, physical time step size
t^*	non-dimensional time step size ($=t/(D/U_b)$)
s, n, z	transformed coordinates
u^+	non-dimensional velocity based on friction velocity
$\bar{u}_i$	filtered velocity
u_iu_j	Reynolds stresses
y^+	non-dimensional wall distance based on friction velocity
x_i	Cartesian coordinate $i = 1, 2, 3$
A, B, C	coefficients
C_w	subgrid-scale model coefficient
D	width of the duct
L	larger turbulent length scale ($=k^{3/2}/\varepsilon$)
$\bar{p}$	filtered pressure
R_c	curvature radius
Re	Reynolds number ($=U_bD/\nu$)
R_o	rotation number ($=\Omega D/U_b$)
RMS	root mean square
$\overline{S}_{ij}$	resolved-scale strain rate tensor
SGS	subgrid-scale
T	time scale of larger eddies ($=k/\varepsilon$)
U_i	mean (or time-averaged) velocity
U_b	streamwise bulk velocity

Greek symbols

Δ_{ij}	Kronecker-delta ($=1$ if $i=j$, $=0$ otherwise)
ε	dissipation rate of turbulent kinetic energy
ϕ	bend angle
η	Kolmogorov scale ($=(\nu^3/\varepsilon)^{1/4}$)
λ	Taylor length scale ($=(10\nu k/\varepsilon)^{1/2}$)
λ_t	Taylor time scale ($=(15\nu/\varepsilon)^{1/2}$)
ν	kinematic viscosity
ν_t	subgrid-scale viscosity
τ_{ij}^{SGS}	subgrid-scale stress
Δ	filter width
Ω	rotational speed

Abbreviations

in	inner wall
out	outer wall

The authors believe that there is still a requirement for a clear and unambiguous understanding of the flow physics in U-ducts for design improvements in turbomachinery subjected to strong centrifugal and Coriolis forces. From this standpoint, the primary goal of the present paper is to validate the LES data for the developing turbulent flow through stationary and rotating U-ducts and to advocate the adoption of LES for such engineering problems.

Numerous experimental and numerical studies have been performed to reveal the flow physics in U-ducts; Azzola et al. (1986), and more recently, Sudo et al. (2000) studied developing turbulent flow experimentally in a U-duct of a circular section. Kikuyama et al. (1994) and Cheah et al. (1996) studied the effect of rotation. Kikuyama et al. (1994) investigated the influence of varying aspect ratios for a low Reynolds number flow in a 90° bend. Cheah et al. (1996) observed that turbulence is damped in the positive rotational case, while it is enhanced in the negative rotational case, aiming to construct a data base for turbulence modelling rather than providing comprehensive flow physics. Iacovides et al. (1996a) and Suga (2003) are among those using algebraic and Reynolds stress model to predict the U-duct flow.

Due to the gradual increase in computational power and efficient use of parallel processing, LES has become an attractive research tool during the last decade or so. However, available LES studies regarding the U-duct are quite scarce, probably due to the complexity of the geometry. Breuer and Rodi (1994) and Moulinec et al. (2005) have provided the only LES examples regarding mildly curved U-duct flows, and Sewall et al. (2006) along with others focussed on the highly curved square-ended U-duct flows. Recently, several codes have become popular in examining interesting flow problems, thanks to the mesh flexibility and the unstructured solver algorithms contained within. However, these codes require strict validation procedures to deserve consideration for use in design exercises. Thus, prior to a serious attempt regarding the details of the relevant flow physics, the present methodology adopted for the prediction needs to be validated against reliable experimental data. For comparisons, the authors use the data of Cheah et al. (1996), who utilized the Laser Doppler Anemometer (LDA) technique. Their work has also been referenced by many RANS studies, including Iacovides et al. (1996a,b) and Suga (2003).

2. Numerical method

LES is a numerical technique based on resolving the larger scales and modeling the smaller ones. In order to perform this, a filtering operation is needed to isolate the larger scales from the smaller ones. Including the Coriolis force, the filtered continuity and Navier–Stokes equations in tensor notation can be written as:

$$\frac{\partial \bar{u}_i}{\partial x_i} = 0 \tag{1}$$

$$\frac{\partial \bar{u}_i}{\partial t} + \frac{\partial(\bar{u}_i \bar{u}_j)}{\partial x_j} + \in_{ij3} 2\Omega \bar{u}_j = -\frac{1}{\rho}\frac{\partial \bar{p}}{\partial x_i} + \frac{\partial}{\partial x_j}\left(v\frac{\partial \bar{u}_i}{\partial x_j}\right) - \frac{\partial \tau_{ij}^{SGS}}{\partial x_j} \tag{2}$$

The third term on the left hand side of Eq. (2) represents the contribution of the Coriolis force. Centrifugal force is combined with the pressure gradient, since it is conservative in nature. The last term on the right hand side of Eq. (2) represents the subgrid-scale (SGS) stresses, which remain to be modeled. The SGS stress tensor is modeled based on the Bousinesq approach, i.e.,

$$\tau_{ij}^{SGS} - \frac{1}{3}\delta_{ij}\tau_{kk}^{SGS} = -2v_t\overline{S}_{ij} \tag{3}$$

where δ_{ij} is the Kronecker-delta, $\overline{S}_{ij}$ is the resolved-scale strain rate tensor, and v_t is the SGS eddy viscosity. The resolved-scale strain rate tensor is defined as:

$$\overline{S}_{ij} \equiv \frac{1}{2}\left(\frac{\partial \bar{u}_i}{\partial x_j} + \frac{\partial \bar{u}_j}{\partial x_i}\right) \tag{4}$$

In this study, the wall-adapting local eddy-viscosity (WALE) model, proposed by Nicoud and Ducros (1999), is used. Unlike the Smagorinsky model, which was developed by Smagorinsky (1963), this SGS model takes into account both the effects of strain and rotation rates. Thus, the turbulent viscosity has the form:

$$v_t = C_w \Delta^2 \frac{\left(S_{ij}^d S_{ij}^d\right)^{3/2}}{\left(\bar{S}_{ij}\bar{S}_{ij}\right)^{5/2} + \left(S_{ij}^d S_{ij}^d\right)^{5/4}} \tag{5}$$

where

$$S_{ij}^d = \frac{1}{2}\left(\bar{g}_{ij}^2 + \bar{g}_{ji}^2\right) - \frac{1}{3}\delta_{ij}\bar{g}_{kk}^2 \tag{6}$$

and

$$\bar{g}_{ij} = \frac{\partial \bar{u}_i}{\partial x_j} \tag{7}$$

Here Δ is the filter width specified by the cube root of the cell volume and C_w is the model coefficient. The eddy-viscosity, as shown by Eq. (5), goes naturally to zero in the vicinity of a wall so that neither a dynamic procedure nor a damping function is required to capture the proper y^3 wall behaviour. Additionally, the model was seen to handle transition (see Nicoud and Ducros, 1999). Implementation of the model by the same authors for the homogenous isotropic turbulence (HIT) has shown that the model coefficient C_w varies between 0.55 and 0.60 when the WALE model is assumed to have the same ensemble-average subgrid kinetic energy dissipation as the classical Smagorinsky model. Since most of the practical flow problems are inhomogeneous and highly anisotropic, the coefficient C_w should be decreased in a similar fashion as the Smagorinsky model coefficient (C_s). Lilly (1967) derived C_s as 0.18 for HIT; however, it has been commonly used as 0.1 for most of the turbulent flow problems. To account for inhomogeneity and anisotropy in turbulent flow, Temmerman (2004), Fröhlich et al. (2005) and FLUENT (2001) assume the coefficient to be between 0.316 and 0.325. Prior to attempting any of the U-bend simulations, the authors performed a LES of fully developed rotating infinite channel flow at three rotation numbers R_o of 0.05, 0.15 and 0.50 using three SGS models: the WALE model with the coefficient taken as 0.325, the dynamic Smagorinsky model developed by Germano et al. (1991), and the dynamic kinetic energy model developed by Kim and Menon (1995). The LES results were compared with the available DNS data of Kristoffersen and Andersson (1993).

Generally, it was found that the WALE model performed as well as the other models. The most distinct features of the rotating turbulent channel flow – the relaminarization of the flow near the suction side and enhancement of turbulence near the pressure side – were captured acceptably with the WALE model compared to DNS predictions. In addition, this model was found to be computationally less expensive than the other models (around 10% less than the dynamic Smagorinsky model and 20% less than the dynamic kinetic energy model), and was hence chosen for all duct simulations.

It is a common practice to use wall functions to perform LES at a reasonable cost in the case of high Reynolds number and wall-bounded flows (Piomelli and Balaras, 2002). In the current study, the adopted choice is the function based on the work of Werner and Wengle (1991) (WW). Their function assumes a linear-law up to a non-dimensional wall distance (y^+) of 11.81. After this y^+ value, the function uses a power-law description of the form $u^+ = A(y^+)^B$, with $A = 8.3$ and $B = 1/7$. The velocity components tangential to the wall at the grid point next to the wall can be related to the corresponding wall shear stress components by integrating the velocity distribution over the height of the first grid element. This function offers advantages such that no average values are required. Numerical problems in the reattachment regions are also avoided and iterative methods are not required to find the wall shear stress, since an analytical formulation is used to obtain it. In addition, the current wall function was shown to be superior over the classical log-law wall functions due to the integration involved in the implementation (Temmerman, 2004).

In the case of developing turbulent flows, time-dependent inflow boundary conditions are crucially important for LES. In spite of the great efforts expended recently, a prescription of universally accepted inflow condition is still not available. In the present study, a random two-dimensional vortex method proposed by Sergent (2002) was adopted. With this approach, perturbations are added to a specified mean velocity profile via a fluctuating vorticity field (i.e. two-dimensional in the plane normal to the streamwise direction). This vorticity field is generated randomly, but based on the Lagrangian form of the two-dimensional evolution equation of the vorticity and the Biot-Savart law. The vortex particle size is calculated as a form of length scale ($Ck^{3/2}/\varepsilon$, where $C = 0.08$) and is

bounded by the local grid scale in order to ensure that it will always belong to the resolved scales.

Numerical calculations of the filtered governing equations are based on the finite-volume method with an unstructured grid algorithm. For all the calculations, a bounded central differencing scheme, developed by Leonard (1991), is used for the convection term in order to eliminate unphysical wiggles, caused generally when a pure central differencing scheme is chosen. A fully second-order implicit scheme is applied for temporal discretization. The PISO algorithm (Issa, 1986) and PRESTO! scheme (Patankar, 1980) are adopted for the velocity-pressure coupling and pressure interpolation, respectively. Additional information concerning the numerical aspects relevant to the implementation of the LES can be found in the study of Cokljat (1999).

3. Computational domain and flow conditions

LES is known as a grid-dependent technique. The accuracy of LES is improved by explicitly solving for more scales, thereby leaving fewer scales approximated by the SGS models. Increasing the grid resolution also minimizes undesirable effects caused by numerical diffusion. Due to the fact that LES requires fine grid resolution, especially at high Reynolds numbers, it has been regarded as unattractive in many engineering flow calculations. In this paper, the authors attempt to simulate a geometrically difficult flow problem at a high Reynolds number and provide evidence that LES can be relied upon in solving such practical flow problems when the WALE model is coupled with the WW wall function.

Fig. 1a shows the geometrical representation of the flow problem. Developing turbulent flow enters a U-bend of square cross-section with a curvature ratio of $R_c/D = 0.65$ where D is the width of the duct and R_c is the mean curvature radius, i.e. the distance between the curvature axis and the position midway between the inner and outer walls of the bend. Upstream and downstream bend lengths are assumed to be 1.5D and 6D, respectively. The Reynolds number ($Re = U_b D/v$) based on the width of the duct and streamwise bulk velocity is 100,000. Here the bulk velocity is the cross-sectional average of the mean (or time-averaged) streamwise velocity. Two rotational cases are investigated as in the experimental study: one is a positive rotation, where the rotation axis is the same as the curvature axis, and the other is a negative rotation, where the rotation axis is opposite to the curvature axis. It should be noted that the rotational axis is 4.5D away from the bend axis. The rotation number ($R_o = \Omega D/U_b$) is 0.2 in the positive rotational case and -0.2 in the negative rotational case. Here Ω represents the physical

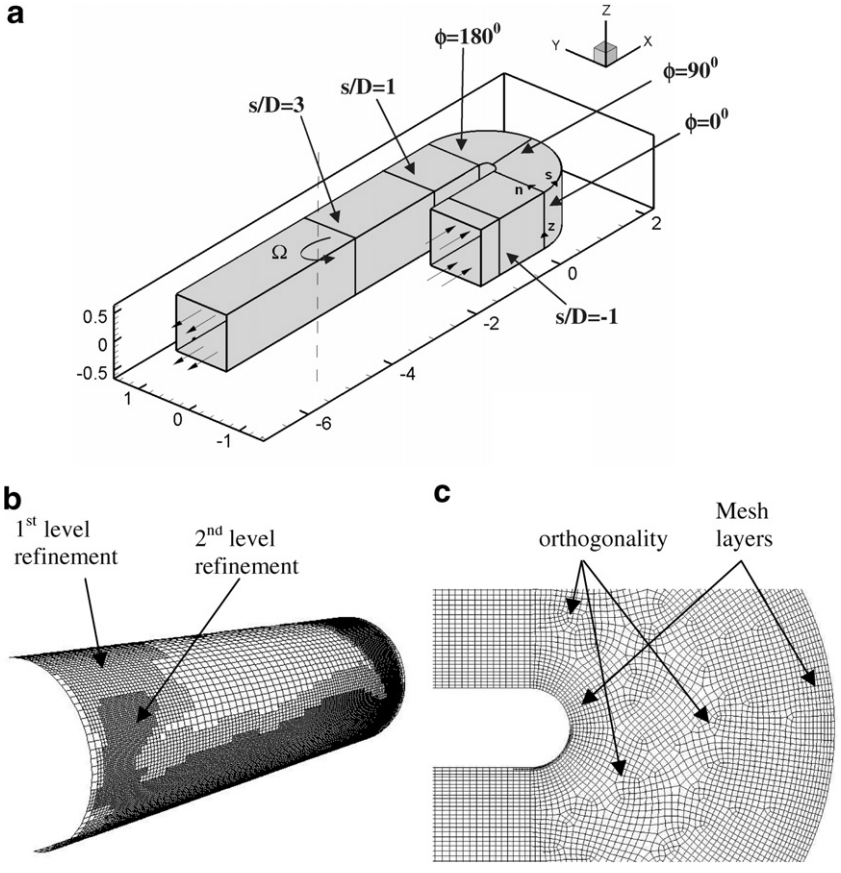

Fig. 1. Geometrical view of U-duct (a). The non-conforming grid distribution on the inner bend wall (b) and the non-orthogonal grid arrangement on the symmetry plane $z/D = 0$ (c).

rotational speed of U-duct. The outer wall becomes the suction side in the positive rotational case and the pressure side in the negative rotational case. Therefore, Coriolis and centrifugal forces reinforce each other in the positive rotational case and oppose each other in the negative rotational case. Non-slip boundary conditions are applied for inner, outer and lateral walls. A preliminary simulation using a Reynolds stress model is performed to find the required three-dimensional velocity profiles (details of which will be given in Section 4.1). At the exit the outflow boundary condition is assumed, resulting in a zero-diffusion flux for all flow variables and in an overall mass balance correction.

In this simulation around 1.1 million cells are used with refinements in the bend. A previous attempt with around 1 million cells with non-adaptive (or non-refined) grid resulted in fully attached flow behaviour near the inner wall, instead of separation. In the case of the non-adaptive grid, where the grid spacing is smoothly increasing or decreasing, high y^+ values appeared due to high velocity gradients. In order to decrease the y^+ values, the non-conforming mesh methodology is used near the high skin friction region. In the current technique, the selected cells in the domain are split into two in every coordinate direction, causing an eightfold increase in total. In some parts of the inner wall of the bend, two levels of refinement were necessary to force the y^+ values to fall in the log-law region (see Fig. 1b). After refinement, y^+ values became less than 35% for 80% of the total grid faces on the walls. Only 5% of the total region employs y^+ values greater than 50, while almost no y^+ values over 70 exist anywhere in the flow domain. This distribution produced significant improvement in the realism of the flow behaviour near the inner bend. In the separation zone, y^+ values are limited to 30. As will be shown later, predictions are in good agreement with the experimental data in the separation region for the cases considered. The non-conforming mesh method has also helped in predicting the accelerated flow behaviour which takes place opposite the separated flow zone.

There are many relevant studies concerning the grid requirements for LES; however, a universally accepted prescription does not exist. It is essential that the resolved turbulent scales have to be in the inertial region of the turbulent kinetic energy spectrum. According to Baggett et al. (1997), the grid filter (Δ) should be at least one-tenth of the larger scales (L). In addition to the larger scales and filter width, Taylor (λ) and Kolmogorov (η) scales are also computed to reveal where the grid filter is located amongst the turbulent length scales. Computations of these scales are performed via the classical k–ε model using the wall functions of Launder and Spalding (1974). As seen in Fig. 2, the grid filter generally lies between the larger scales and the Taylor scales. Here only the mid-point variation for the stationary case is shown, since the overall location of the filter does not change significantly near the walls or for the rotating cases. In the bend a "zigzag" variation of the filter width (Δ) is caused by the non-orthogonal grid topology, a consequence of the adoption of mesh layers

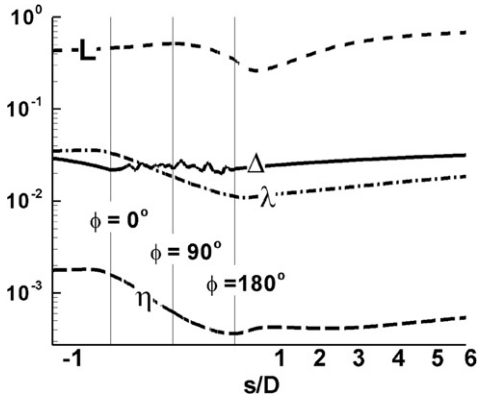

Fig. 2. Grid resolution estimation based on the classical k–ε turbulence model (L, larger scale; Δ, grid filter; λ, Taylor scale; η, Kolmogorov scale).

near the inner and outer walls (Fig. 1c). This could possibly explain to why, to date, LES has not been attempted for a highly curved U-bend flow with rounded inner and outer bend walls. Mildly curved U-bend flow problems allow the users to adopt an equal number of grid points on the inner and outer bend walls, since the order of longitudinal lengths of inner and outer bend walls are close to each other. In the current case the longitudinal length of outer bend wall is around 7.7 times of that of the inner one. In order to avoid highly stretched cells, an adequate number of nodes has to be employed on the outer bend wall based on this ratio. However, it is not feasible to force the grid topology using this high ratio, as this may lead to highly-skewed cells in the middle of the duct. In the light of above discussion, for all the current cases, the grid points on the outer bend wall have been limited to a maximum of three times of that on the inner bend, thus a reasonable level of cell skewness is achieved in the centre of the geometry.

4. Results

In the current numerical study, LES predictions are compared with the experimental data of Cheah et al. (1996) and the RANS data of Suga (2003) who conducted several RANS simulations and concluded that only Craft and Launder (1996) two-component-limit (TCL) model can be relied upon for the U-duct flow. Therefore, in the current paper the TCL model has been referenced for comparisons along with the experimental data. Since Suga (2003) performed only stationary U-bend simulation, LES and RANS comparisons could be made only for the stationary case. Comparisons include primary and secondary velocities, turbulent intensities and primary turbulent shear stresses. The measurements were taken both on the "symmetry" plane (or mid-span plane, $z/D = 0$) of the duct and on the "top" plane which is located 12.5% away from the top lateral wall ($z/D = +0.375$).

Discretization of Eqs. (1) and (2) leads to a solution methodology based on a Cartesian coordinate system regardless of the imported grid topology. In order to

perform proper comparisons with experimental data, these instantaneous Cartesian velocity components are transformed to streamwise, wall-normal (or radial) and spanwise velocity components at every time step and the statistics are collected based on the transformed velocities using separate user defined subroutines explicitly implemented in the code. The simulations are performed using a non-dimensional time step ($t^* = t/(D/U_b)$) of 0.002, where t is the physical time step. This time step was chosen such that the time scale of the resolved eddies is far less than the timescale of larger eddies ($T = k/\varepsilon$) and close to the timescale of smaller eddies (Taylor timescale, $(\lambda_t = 15\nu/\varepsilon)^{1/2}$; for more information refer to Pope (2000)). The minimum values of T and λ_t are found to be 0.252 and 0.029, respectively in non-dimensional time units. The chosen non-dimensional time step of 0.002 is even less than λ_t, due to the embedded mesh refinement. Residuals of continuity and Cartesian velocities at every time step are reduced to less than 10^{-3} and 10^{-5}, respectively. For all the cases, around 20,000 time steps are performed to complete the statistics. This number corresponds to 40 letots (large-eddy turnover time $= D/U_b$). All the calculations were performed using one P4 Intel 3.00 GHz processor with 2 GB memory capacity. Around 2.5 min were needed for one time step, allowing the collection of the turbulent statistics to be completed in approximately one month.

4.1. Implementation of the inlet boundary condition

The main difficulty in this study has been the implementation of the inlet boundary condition. Lack of experimental measurements well upstream of the bend forced the authors to find a reasonable three-dimensional mean velocity profile by which the predictions at the bend inlet could be matched with the experimental data.

First, a developing turbulent flow is solved using the Reynolds stress model described by Launder et al. (1975) for a long straight square duct (20D) with the same cross-sectional area and the Reynolds number as that of the U-duct. A boundary layer thickness of 2% of the duct width and a turbulent intensity of 1% of the bulk velocity are assumed for the inlet boundary condition for this auxiliary RANS simulation. The predictions on the symmetry plane at certain stations between 5D and 15D are compared with the experimental data, which was measured three diameters upstream of the bend-inlet. The final inlet velocity profile for LES is assumed to be the one that is 1.5 diameters away from the station where the predicted boundary layer thickness is almost the same as the experiment both at the inner and outer walls. The predicted turbulent kinetic energy (k) and the dissipation rate of the turbulent kinetic energy (ε) at the corresponding station were used as inputs for the random vortex perturbation method in order to estimate the size and location of the vortex. Then, as explained in detail in Sergent (2002), the vortices are distributed randomly via a spatial-distribution function η:

$$\eta(\vec{z}) = \frac{1}{2\pi\sigma^2}\left(2e^{-|z|^2/2\sigma^2} - 1\right)2e^{-|z|^2/2\sigma^2} \tag{8}$$

with a circulation Γ:

$$\Gamma(z,y) = 4\sqrt{\frac{\pi A k(z,y)}{3N[2\ln(3) - 3\ln(2)]}} \tag{9}$$

where A and N denote the area of the inlet section and the number of vortex points that can be controlled by the user.

As noted earlier, the inlet is taken as 1.5 diameters downstream of the bend inlet. Unfortunately, experimental data is not available at this station. In order to have an idea of how well the velocity profile is mimicked, the authors compare LES predictions to the measurements at the bend inlet as shown in Fig. 3. Following a similar velocity profile being adopted at $s/D = -1.5$ for the stationary and positive rotational cases, the agreement between experiment and LES at the bend inlet is seen to be quite good apart from a slight discrepancy for the stationary case near the outer wall. This discrepancy might be due to variability of the boundary layer thickness near the inner and outer walls, which was interpreted from the experimental data at $s/D = -3$. Unfortunately, for the stationary case, this uneven boundary layer thickness at the walls could not be produced from the preliminary straight duct simulation. For the negative rotational case, another preliminary simulation is performed by incorporating a rotational number of $R_o = -0.2$ using the same procedure followed for the stationary case to obtain the velocity profile. The final velocity profile configuration also yields satisfactory results at bend inlet both near the inner and outer walls (similar to the other cases). Based on the results in Fig. 3, the authors concluded that the adopted inlet mean velocity profile is reasonable for all the cases, since the acceleration and deceleration of the flow near the inner and outer walls around the bend inlet are very well captured without significant discrepancies between the experimental data and predictions.

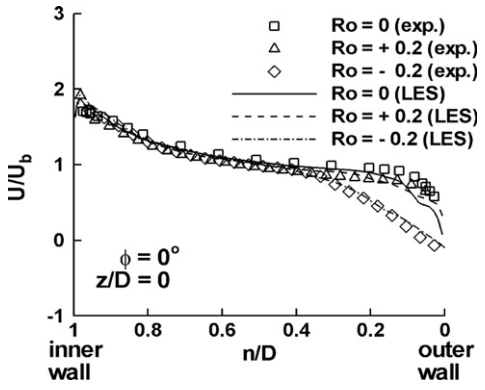

Fig. 3. Comparisons of the mean streamwise velocity predictions and measurements at the bend inlet $\phi = 0°$.

4.2. Primary velocity predictions

Mean streamwise velocity comparisons are shown in Fig. 4. At the half-bend station, $\phi = 90°$, streamwise velocity predictions show that the separation zone is predicted to be thinner than the measurements, which might indicate that separation takes place later than the experiments. Yet, this does not have an adverse effect on the overall predictions of the details of the separation region, which is quite different than the RANS behaviour. The TCL model does perform well at $\phi = 90°$, but under-predicts the size and the magnitude of the separation region at $\phi = 180°$ (Fig. 4a). The separated region is further reduced at the top plane (Fig. 5). Here LES predictions of the separation region are improved compared to the symmetry plane $z/D = 0$ due to the relatively fine grid near the lateral walls of the duct.

At the exit of the bend, $\phi = 180°$, LES predictions are in good agreement with the experimental data despite some discrepancies at the symmetry plane for the stationary case (Fig. 4a) and at the top plane for the negative rotational case (Fig. 5c). As was mentioned earlier for $\phi = 90°$, these discrepancies are thought to be mainly caused by inadequate prediction of the separation zone details. Although

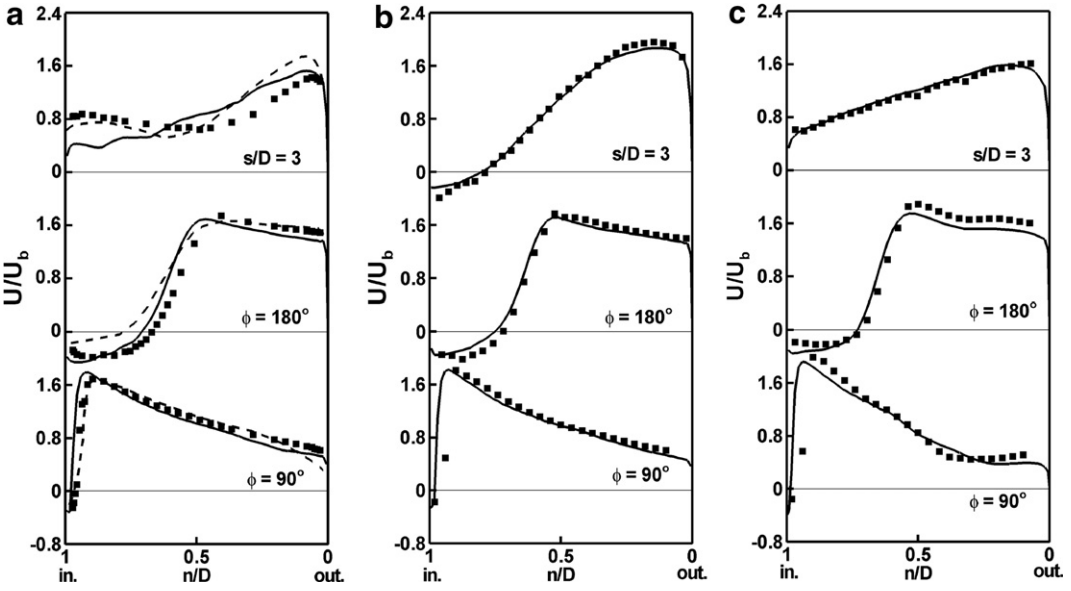

Fig. 4. Mean streamwise velocity comparisons on the symmetry plane $z/D = 0$ for $R_o = 0$ (a), $R_o = +0.2$ (b) and $R_o = -0.2$ (c) (■■ experiment, — LES, --- TCL).

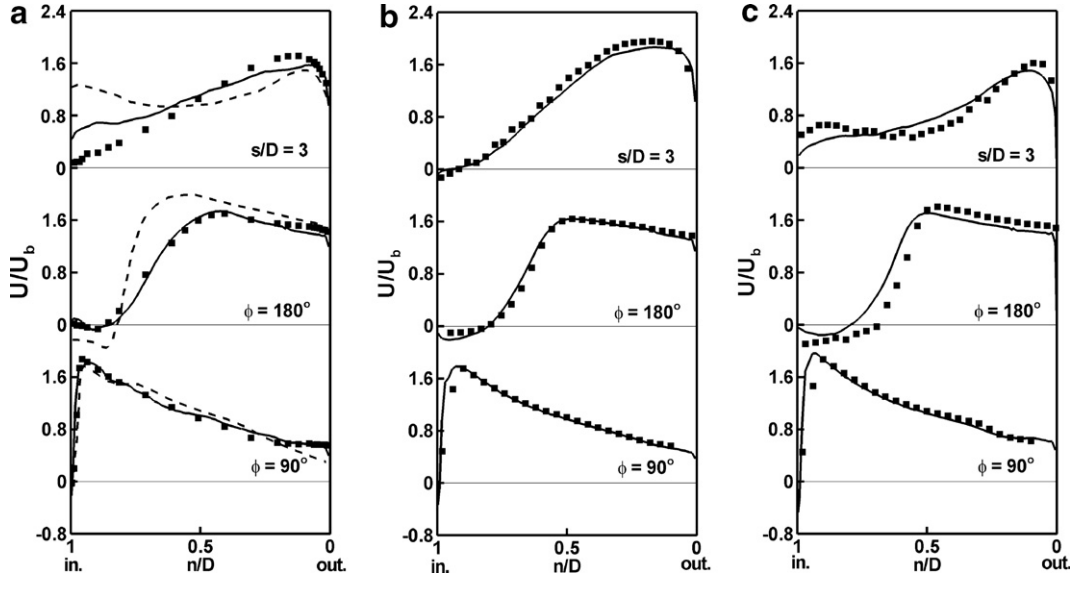

Fig. 5. Mean streamwise velocity comparisons on the top plane $z/D = 0.375$ for $R_o = 0$ (a), $R_o = +0.2$ (b) and $R_o = -0.2$ (c) (■■ experiment, — LES, --- TCL).

it is not shown here due to space limitations, it is appropriate to mention that the discrepancies for the predicted mean streamwise velocity are observed to be closely related to those for the predicted mean wall-normal velocity, especially for the inner half of the bend. This would suggest that the numerical method that is used to resolve or model the separation region is crucially important regarding the accurate predictions of primary and secondary velocities, and hence the turbulent intensities, as the authors discuss in the following section.

At the last station, $s/D = 3$, LES predictions (Figs. 4 and 5) are in very good agreement with the experimental data for the rotational cases. However, the same comments cannot be made for the stationary case for either LES or the TCL model (see Figs. 4a and 5a). For LES cases this is a paradox, since the rotational cases would naturally provide a more challenging problem due to the fact that the Coriolis effects must also be taken into account. Streamwise velocities are under-predicted at the symmetry plane near the inner wall, whereas they are over-predicted at the top plane near the same wall. The origin of these discrepancies is most probably the slight over-prediction at the bend exit, where the rotational case predictions coincide with the experimental data. Even though it is not shown here, these over-predictions become more significant downstream of the bend without any detrimental influence on the separated region details. After the separation region, recovery becomes slower near the inner wall, corresponding to over-predictions near the outer wall. In order to satisfy the continuity criterion, a slower recovery at the symmetry plane is accompanied by a faster recovery near the top plane. This problem is aggravated with the TCL model such that predictions become approximately 120% off the experimental values near the inner wall (see Fig. 5a). LES is very sensitive to boundary conditions and is always a "grid-dependent" technique, therefore the authors are of the opinion that the discrepancies of the streamwise velocities at $s/D = 3$ might be due to an insufficient grid resolution near this station or slight inaccuracies in mimicking the inlet velocity profile.

4.3. Turbulence predictions

RMS values of streamwise and wall-normal velocity fluctuations are displayed in Figs. 6 and 7. While the flow separates around the half-bend, strong turbulence is generated near the inner bend. Similar to the mean streamwise predictions, the RMS values of streamwise velocity fluctuations for the station $\phi = 90^\circ$ are predicted very well by LES for all cases except for the stationary case. Discrepancies between LES and experiments might be due to the particular perturbation method adopted and/or the relatively larger grid cells employed. The perturbations develop very quickly within a short distance and cause high RMS levels, hence LES usually over-predicts RMS values near the outer wall. For the rotational cases, such adverse effects are not observed since rotation becomes a dominant factor in governing the velocity fluctuations; the Coriolis force leads to suppression of the turbulence in the positive rotation mode and to an increase in turbulence for the negative rotation mode. It is quite possible that the under-predictions near the inner wall could be due to inadequate grid resolution rather than to the inlet perturbations. Similar to what was observed in Fig. 6, RMS values of wall-normal velocity fluctuations are under-predicted near the inner bend and over-predicted near the outer bend, as shown in Fig. 7. This is a common problem in LES, for which fine grid resolution is needed near the walls in order to capture the wall-normal turbulent stresses accurately. In the cur-

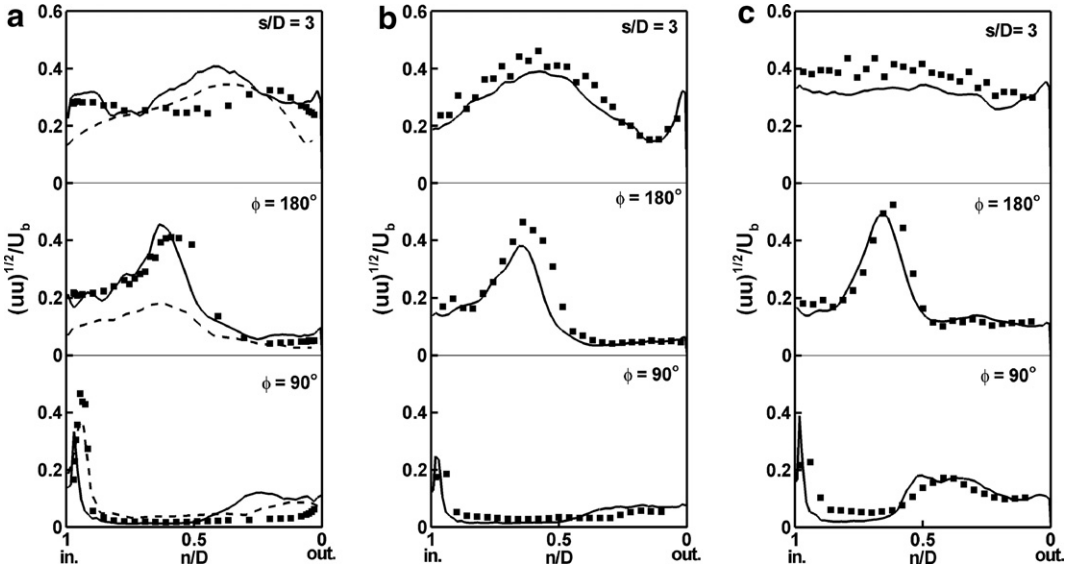

Fig. 6. RMS comparisons of streamwise velocity fluctuations on the symmetry plane $z/D = 0$ for $R_o = 0$ (a), $R_o = +0.2$ (b) and $R_o = -0.2$ (c) (■■ experiment, — LES, --- TCL).

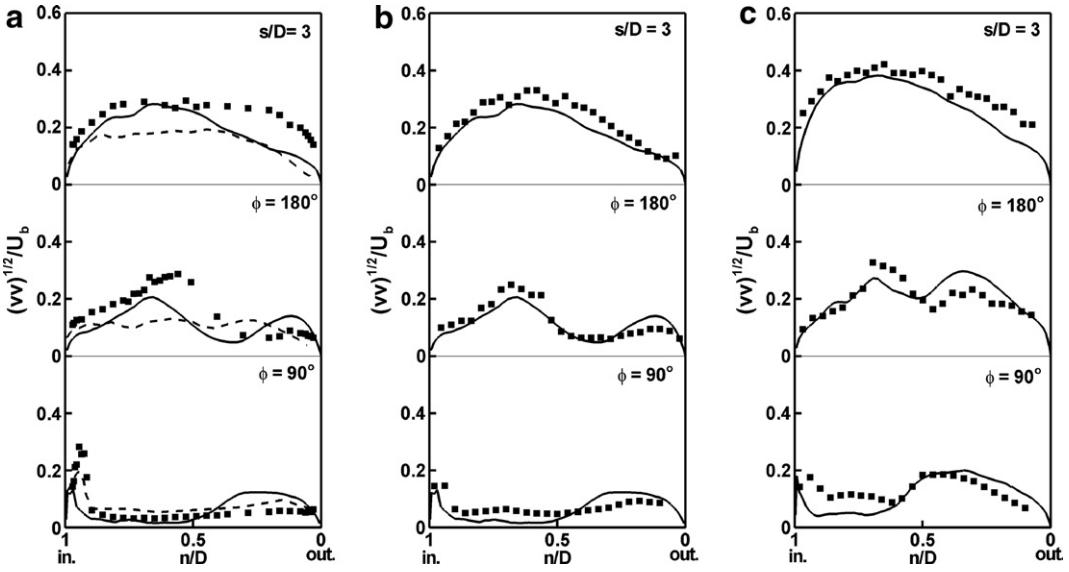

Fig. 7. RMS comparisons of wall-normal velocity fluctuations on the symmetry plane $z/D = 0$ for $R_o = 0$ (a), $R_o = +0.2$ (b) and $R_o = -0.2$ (c) (■■ experiment, — LES, --- TCL).

rent study, further grid refinement could not be performed to resolve this problem since two level refinements had already been performed as seen in Fig. 1b. Hence another refinement for that region would have substantially increased the demand for computational power. The TCL model does a rather better job than LES at $\phi = 90^\circ$ near the inner and outer walls in predicting the RMS values, which is attributed to slight coarse grid topology adopted for these local regions in LES simulations.

At $\phi = 180^\circ$ and $s/D = 3$, LES performs much better than the TCL model in predicting the RMS values of velocity fluctuations (Figs. 6a and 7a), corresponding to the streamwise velocity predictions (Figs. 4a and 5a). At this station the mean flow is comprised of three regions: a separated region near the inner wall, an accelerated region near the outer wall and a shear region between these regions. Corresponding to this classification, the RMS values of streamwise velocity fluctuations reaches a high-level of 0.5–0.6 in the shear region, a medium-level of around 0.2 in the separation region and a low-level of around 0.1 in the accelerated region. This turbulence behaviour is very well captured by LES for all cases. However, the TCL model under-predicts significantly the level of RMS values and fails in capturing the true trends (see Figs. 6a and 7a).

At $s/D = 3$, encouraging results by LES are obtained for the rotational cases. The discrepancies for the stationary case are attributed to the inaccuracies in predictions of the mean streamwise velocity. The TCL model, on the other hand, significantly under-predicts the RMS values of streamwise velocity fluctuations near the walls, but produced slightly better results than LES for $0.4 < n/D < 0.7$.

The primary turbulent shear stress can be taken as the time-averaged correlation of streamwise and wall-normal velocity fluctuations. Significant turbulent shear stress variations are only observed after the bend exit. As seen in Fig. 8, these turbulent stresses are reasonably predicted by LES. However, the shear stress levels reported for the TCL model are seriously too low. The authors think that for more accurate turbulent shear stress predictions, special care has to be taken of the grid resolution for the LES simulations; Discrepancies between LES and experiments are diminished while approaching the top plane where a relatively finer grid is used in comparison to the symmetry plane.

4.4. Further physical considerations

This section considers briefly some relevant flow physics which have not been documented explicitly in the past

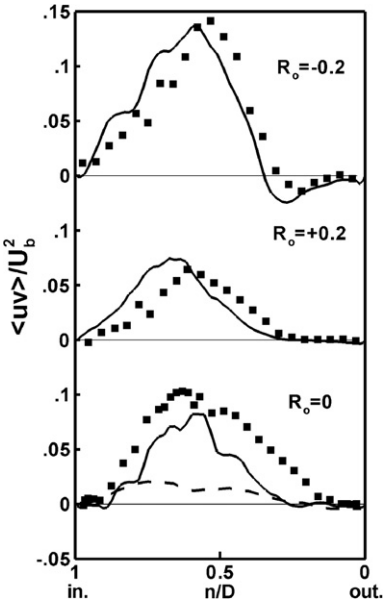

Fig. 8. Primary turbulent shear stress comparisons on the symmetry plane $z/D = 0$ at $s/D = 1$ (■■ experiment, — LES, --- TCL).

regarding this particular flow problem. Fig. 9 illustrates the mean primary flow on the symmetry plane (Fig. 9a) and the secondary flow at the exit of the bend (Fig. 9b). From the inlet up to the end of the bend, the primary flow does not seem to differ significantly among the test cases. However, it is noted that the separation lasts longer for the positive rotational case after the bend. This is due to the fact that the Coriolis force acts from the inner to the outer wall on the mean streamwise flow, thus enhancing the separation region. On the other hand, the separation region is shortened in the negative rotational case, where the Coriolis force acts in the reverse direction. Corresponding to the thicker separation region, the flow accelerates more near the outer wall for the positive rotational case compared with the other cases.

The secondary flow (Fig. 9b) has similar characteristics for the stationary and positive rotational cases, where the flow tends to move from the inner to the outer wall. It is seen that there are two identical, relatively thin vortices sitting near the lateral walls for the stationary case. These vortices disappear in the positive rotational case due to increased flow displacement from the inner to the outer wall caused by the Coriolis force. In the negative rotational case, since the Coriolis force counteracts the centrifugal force, the flow changes sign, being directed from the outer to the inner wall. Thus, due to these two opposing flows, a large vortex pair is formed near the outer wall, accompanied by another vortex pair appearing at the inner wall.

Fig. 10a demonstrates the positive (rendered by light grey) and the negative (rendered by black) iso-values of mean streamwise vorticity. This would suggest that the mean secondary flows are rotating in clockwise (light grey structures) and anti-clockwise (black structures) directions. At the inlet, some thin vortex tubes exist due to long time statistics of the random vortex motion. After the bend, as discussed in the previous paragraph, there is a long thin vortex placed near the lateral wall. A relatively larger vortex, placed under the thin vortex, can also be seen in

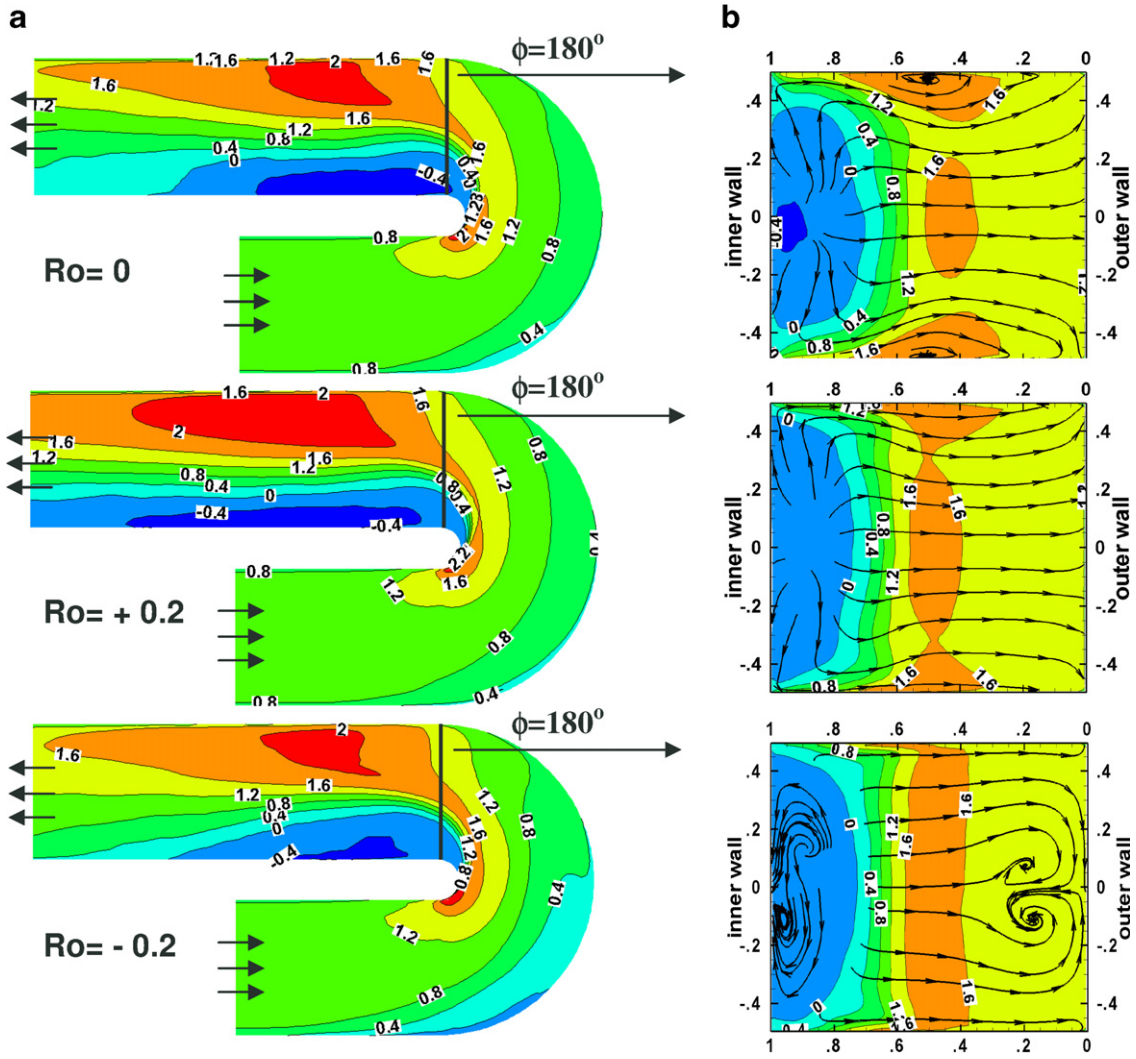

Fig. 9. Mean streamwise velocity contours (U/U_b) at the symmetry plane $z/D = 0$ (a) and the bend exit $\phi = 180^\circ$ (b), where the secondary flow behaviour is also shown.

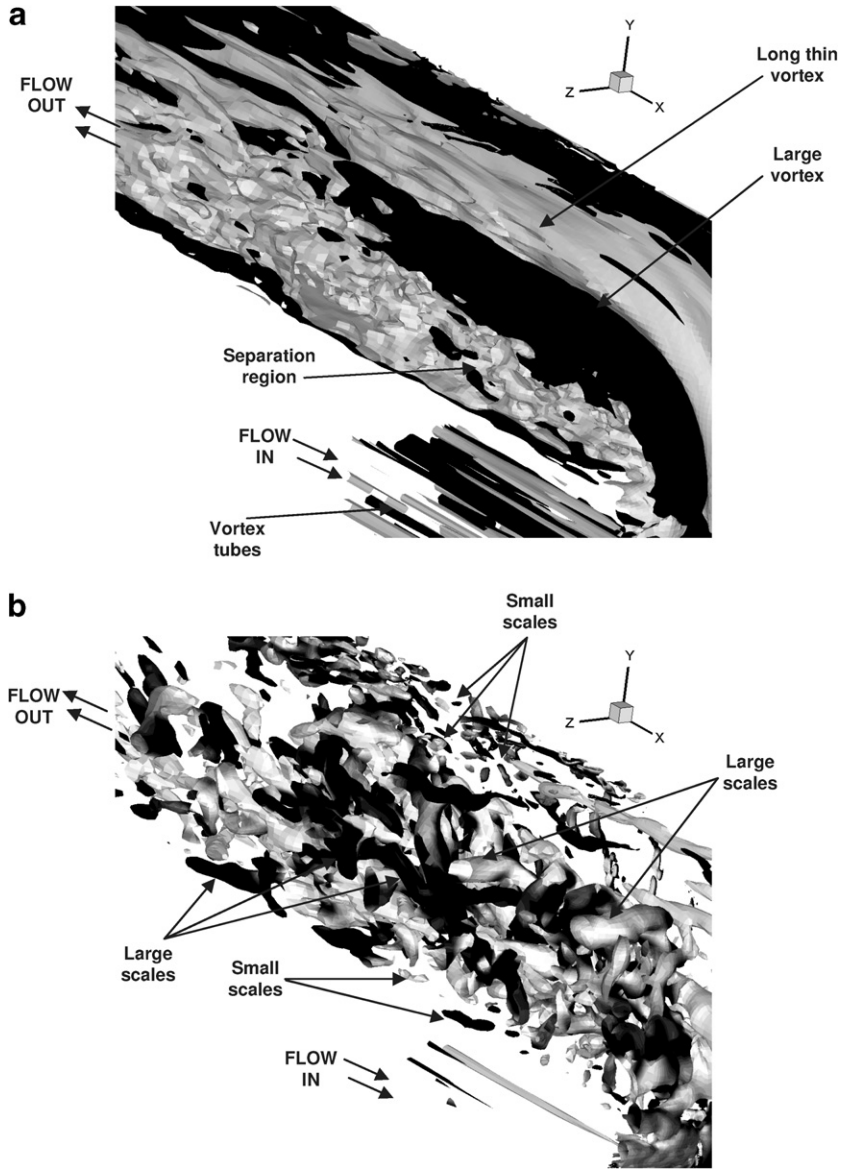

Fig. 10. Mean iso-values of streamwise vorticity (a) and instantaneous flow structures determined by Q-criterion (b) for stationary case. Mean (a) and instantaneous (b) vortex motion is represented by clockwise (coloured by light grey) and anti-clockwise (coloured by black) direction. Due to sake of clarity, only half of the geometry ($z/D < 0$) is shown.

Fig. 10a. A detailed discussion on the behaviour of the secondary flow is planned in a separate study.

One of the advantages of performing LES is to reveal the coherent structures, features of which might not be properly resolved from experiments or from RANS. Coherent structures are calculated via the Q-criterion, proposed by Hunt et al. (1988). It is based on the calculation of the second invariant of the velocity gradient tensor and it was shown by the same authors that only positive Q-values represent the true structures. In Fig. 10b, the iso-values of Q, for which the threshold is taken as $20(U/D)^2$ in order to distinguish larger scales from smaller ones, are shown and rendered by contours of instantaneous streamwise vorticity. It is thus possible to identify smaller and larger structures which may rotate clockwise (light grey) or anti-clockwise (black). It is worth noting that most of the captured small scales occur near the separation (low-momentum) and outer wall (high-momentum) regions. In the middle of the duct, anti-clockwise rotating structures are more dominant, which can also be regarded as the instantaneous field of the mean large vortex shown in Fig. 10a.

5. Conclusions

In this paper, a large-eddy simulation of the developing turbulent flow subject to strong centrifugal and Coriolis forces through a U-duct at a high Reynolds number has been presented. The main aim has been to show the experimental validation of the LES predictions for the first time in the literature for this particular flow case. In spite of the high Reynolds number and limited experimental

information about the inlet velocity profiles, the agreement between the predictions and corresponding experimental data is generally satisfactory.

Discrepancies between the predictions and the experimental data are thought to be due to the combined effect of the grid resolution, the wall function, the inlet velocity profile and the experimental uncertainties (especially the ones regarding the turbulence). Grid resolution is thought to have some effects on the profiles of Reynolds stresses. The wall function is generally believed to be mainly responsible for the excessive turbulent intensities, which were seen particularly upstream of the half bend at the symmetry plane for the stationary case.

Current LES predictions are also compared with the two-component-limit turbulence model for this particular U-duct flow problem by Suga (2003). Generally, LES was seen to be superior to two-component-limit turbulence model with regard to the predictions of mean velocities and for turbulent stresses. Inaccuracies of LES at the half-bend station are attributed to grid resolution.

The authors plan to perform a comprehensive analysis of the flow physics based on these validated results. The investigation of the primary and secondary flow behaviour based on a cross-sectional view would suggest a better understanding of the origin and development of the flow separation. It is also of interest to see how the centrifugal and the Coriolis forces affect the turbulence in the bend as well as downstream of the bend.

Acknowledgements

The authors thank Prof. H. Iacovides for providing the experimental data. The authors are also grateful for the comments and suggestions of a referee and the Editor. In addition, K.M. Guleren thanks the Turkish Government for the scholarship and the Cumhuriyet University for a leave of absence to carry out PhD studies at the University of Manchester. The simulations were performed in the computational laboratory of the Power Generation Group in the School of MACE, the University of Manchester.

References

Azzola, J., Humphrey, J.A.C., Iacovides, H., Launder, B.E., 1986. Developing turbulent flow in a U-bend of circular cross-section: measurement and computation. J. Fluid. Eng. 108, 214–221.

Baggett, J.S., Jimenez, J., Kravchenko, A.G., 1997. Resolution Requirements in Large-eddy Simulations of Shear Flows, Annual Research Briefs. Center for Turbulence Research, Stanford University, Stanford, USA.

Breuer, M., Rodi, W., 1994. Large-eddy simulation of turbulent flow through a straight square duct and 180° bend, Fluid Mechanics and its Applications, Selected Papers from the First ERCOFTAC Workshop on Direct and LES, Guildford, Surrey, UK, 27–30 March, Voke, Kleiser, Chollet (Eds.), Direct and Large-Eddy Simulation I, vol. 26, pp. 273–285, Kluwer Academy Publisher.

Cheah, S.C., Iacovides, H., Jackson, D.C., Ji, H., Launder, B.E., 1996. LDA investigation of the flow development through rotating U-ducts. J. Turbomach. 118 (3), 590–596.

Cokljat, D., 1999. Large-eddy simulation of flow around surface-mounted cubical obstacles, Part I: Numerical Aspect. LESFOIL Project Report. Fluent Europa Ltd., Sheffield, UK.

Craft, T.J., Launder, B.E., 1996. A Reynolds-stress closure designed for complex geometries. Int. J. Heat Fluid Flow 17, 245–254.

FLUENT 6.2 User Guide, 2001. Fluent Inc., Lebanon, USA.

Fröhlich, J., Mellen, C.P., Rodi, W., Temmerman, L., Leschziner, M.A., 2005. Highly resolved large-eddy simulation of separated flow in a channel with streamwise periodic constrictions. J. Fluid Mech. 526, 19–66.

Germano, M., Piomelli, U., Moin, P., Cabot, W.H., 1991. A dynamic subgrid-scale eddy viscosity model. Phys. Fluids. 7, 1760–1765.

Hunt, J.C.R., Wray, A.A., Moin, P., 1988. Eddies, stream, and convergence zones in turbulent flows, Report CTR-S88. In: Proceedings of the 1988 Summer Program, Stanford N.A.S.A Center For Turbulence Research.

Iacovides, H., Launder, B.E., 2006. Internal blade cooling: the cinderella of turbomachinery C&EFD research in gas turbines, Invited Paper, 13th International Heat Transfer Conference, Sydney.

Iacovides, H., Launder, B.E., Li, H.-Y., 1996a. The computation of flow development through stationary and rotating U-ducts of strong curvature. Int. J. Heat Fluid Flow 17, 22–33.

Iacovides, H., Launder, B.E., Li, H.-Y., 1996b. Application of a reflection-free DSM to turbulent flow and heat transfer in a square-sectioned U-bend. Exp. Therm. Fluid Sci. 13, 419–429.

Issa, R.I., 1986. Solution of implicitly discretized fluid flow equations by operator splitting. J. Comput. Phys. 62, 40–65.

Kikuyama, K., Maeda, T., Yokoi, T., 1994. Turbulent flows inside a rotating curved rectangular channel for different aspect ratios. Exp. Therm. Fluid Sci. 9, 215–224.

Kim, W.W., Menon, S., 1995. A New Dynamic One-equation Subgrid-scale Model for Large Eddy Simulations. AIAA-95-0356.

Krain, H., 2005. A review of centrifugal compressor's application and development. J. Turbomach. 127 (1), 25–34.

Kristoffersen, R., Andersson, H.I., 1993. Direct simulations of low-Reynolds-number turbulent-flow in a rotating channel. J. Fluid Mech. 256, 163.

Launder, B.E., Spalding, D.B., 1974. The numerical computation of turbulent flows. Comput. Meth. Appl. Mech. Eng. 3, 269–289.

Launder, B.E., Reece, G.J., Rodi, W., 1975. Progress in the development of a Reynolds-stress turbulence closure. J. Fluid Mech. 68, 537–566.

Leonard, B.P., 1991. The ULTIMATE conservative difference scheme applied to unsteady one-dimensional advection. Comput. Meth. Appl. Mech. Eng. 88, 17–74.

Lilly, D.K., 1967. The representation of small-scale turbulence in numerical simulation experiments. In: Proceedings of the 10th Scientific Computing Symposium on Environmental Sciences, Yorktown Heights, NY, IBM, pp. 195–210.

Moulinec., C., Benhamadouche, S., Laurence, D., Perić, M., 2005. LES in a U-bend pipe meshed by polyhedral cells. In: Engineering Turbulence Modelling and Measurements, Sardinia, Italy. 23–25 May.

Nicoud, F., Ducros, F., 1999. Subgrid-scale stress modelling based on the square of the velocity gradient tensor. Flow, Turbul. Combust. 62 (3), 183–200.

Patankar, S.V., 1980. Numerical Heat Transfer and Fluid Flow. Hemisphere, Washington, DC.

Piomelli, U., Balaras, E., 2002. Wall-layer models for large-eddy simulations. Ann. Rev. Fluid Mech. 34, 349–374.

Pope, S.B., 2000. Turbulent Flows. Cambridge University Press.

Sergent, E., 2002. Vers une methodologie de couplage entre la Simulation des Grandes Echelles et les modeles statistiques, PhD thesis, L'Ecole Centrale de Lyon, Lyon, France.

Sewall, E.A., Tafti, D.K., Graham, A.B., Thole, K.A., 2006. Experimental validation of large eddy simulation of flow and heat transfer in a stationary ribbed duct. Int. J. Heat Fluid Flow 27, 243–258.

Smagorinsky, J., 1963. General circulation experiments with primitive equations. I. The basic experiment. Monthly Weather Rev. 91, 99.

Sudo, K., Sumida, M., Hibara, H., 2000. Experimental investigation on turbulent flow through a circular-sectioned 180° bend. Exp. Fluids 28, 51–57.

Suga, K., 2003. Predicting turbulence and heat transfer in 3-D curved ducts by near-wall second moment closures. Int. J. Heat Mass Transfer 46, 161–173.

Temmerman, L., 2004. Large Eddy Simulation of Separating Flows from Curved Surfaces, PhD thesis, Queen Mary University of London, London, UK.

Werner, H., Wengle, H., 1991. Large-eddy simulation of turbulent flow over and around a cube in a plane channel. In: Eighth Symposium on Turbulent Shear Flows, Munich, Germany.